On a solution reconstruction and limiting procedure for unstructured finite volumes

Conference Paper · May 2014

2 authors:

Argiris Delis
Technical University of Crete

Ioannis K Nikolos
Technical University of Crete

Manuscript submitted to
AIMS' Journals
Volume **X**, Number **0X**, XX **200X**

Website: http://AIMsciences.org

pp. **X–XX**

ON A SOLUTION RECONSTRUCTION AND LIMITING PROCEDURE FOR UNSTRUCTURED FINITE VOLUMES

A.I. Delis

Department of Sciences, Division of Mathematics,
Technical University of Crete, University Campus,
Chania, Crete 73100, Greece

I.K. Nikolos

Department of Production Engineering & Management,
Technical University of Crete, University Campus
Chania, Crete 73100, Greece

Abstract. The present paper deals with the continuous work of extending the application of a multidimensional-type solution reconstruction and limiting procedure into the finite volume (FV) computation of 2D compressible flows. Based on a MUSCL-type technique, this reconstruction procedure identifies and cures poor connected grids without suffering from loss of accuracy by taking into account geometrical characteristics of computational triangular and hybrid meshes and is independent of the Riemann solver used. Monotonicity in the solution is enforced by a limiting strategy that implements well-known edge-type limiters hence avoiding the procedure of solving any minimization problems. Through several test cases, it is observed that the methodology provides quite desirable performances in retaining the formal order of accuracy, controlling numerical oscillations as well as capturing key flow features.

1. **Introduction.** In multidimensional high-resolution FV schemes, on unstructured meshes, numerous solution reconstruction and limiting strategies have been developed to resolve complex flows. Many of these strategies involve the construction of an appropriate linear representation of the solution variables within each FV element, which is then limited as to enforce positivity and stability constraints on the scheme, usually based on the satisfaction of the Maximum Principle [4]. Although current reconstruction and limiting methods have enjoyed success in many CFD applications, there is no consensuses on a global optimal reconstruction strategy that fulfills a high-level of accuracy, robustness and convergence. As such, the search for efficient reconstruction and limiting processes, in a multidimensional context, is still an active field of research, see for example [1, 6, 5, 3] and references therein. Recently, in [2] and [3], a cell-centered finite volume (CCFV) scheme of the Godunov-type with a novel solution reconstruction and limiting procedure was developed and tested for smooth and non-smooth shallow water flow computations. This novel alternative procedure was developed in order to apply in the reconstruction an edge-based limiting strategy that takes into account geometrical characteristics of the computational mesh. Grids with poor connectivity [4, 1], i.e.

2000 *Mathematics Subject Classification.* Primary: 65M08, 70M12; Secondary: 35L65.
Key words and phrases. Finite volumes, linear reconstruction, limiting, Euler equations.

those whose flux integration points do not coincide with the location to which reconstructed values are computed, can be properly treated. The use of edge-type limiters avoids the procedure of solving any minimization problems or the need to use any tunable parameters.

In this presentation, the reconstruction and limiting procedure proposed in [2, 3] is applied to the approximation of the Euler equations and compares its performance when implementing truly multidimensional limiters. Two well-known approximate Riemann solvers are implemented, demonstrating the procedure's independence to the solver used, as well as its universal applicability, efficiency and robustness to either conservative or primitive variable reconstructions. Its applicability to some node-centered (vertex-centered) FV schemes is also briefly sketched.

2. **The Euler equations.** In their conservative form the 2D Euler equations read as

$$\partial_t \mathbf{U} + \nabla \cdot \mathcal{H}(\mathbf{U}) = 0 \quad \text{on} \quad \Omega \times [0,t] \subset \mathbb{R}^2 \times \mathbb{R}^+, \tag{1}$$

where $\Omega \times [0,t]$ is the space-time Cartesian domain over which solutions are sought, $\mathbf{U}$ is the vector of the conserved variables and $\mathcal{H} = [\mathbf{F}, \mathbf{G}]$ are the nonlinear flux vectors defined as

$$\mathbf{U} = \begin{bmatrix} \rho \\ \rho u \\ \rho v \\ \rho e_T \end{bmatrix}, \quad \mathbf{F}(\mathbf{U}) = \begin{bmatrix} \rho u \\ \rho u^2 + p \\ \rho u v \\ (\rho e_T + p) u \end{bmatrix}, \quad \mathbf{G}(\mathbf{U}) = \begin{bmatrix} \rho v \\ \rho u v \\ \rho v^2 + p \\ (\rho e_T + p) v \end{bmatrix}. \tag{2}$$

Here, ρ is the flow density, p is the flow pressure, e_T is the specific total energy, and $\mathbf{u} = [u, v]^{\mathrm{T}}$ are the velocity components. The system is completed by the equation of state for a perfect gas, $p = (\gamma_s - 1)\left(\rho e_T - \frac{1}{2}\rho \|\mathbf{u}\|^2\right)$, where $\gamma_s = 1.4$ is the ratio of the specific heats. Hyperbolic system (1) is supplemented by the initial condition $\mathbf{U}(x, y, 0) = \mathbf{U}_0(x, y)$, $x, y \in \Omega$ and by appropriate boundary conditions (periodic, inflow, outflow, slip) on the boundary $\partial\Omega$ of Ω.

3. **FV framework and the MUCL-type reconstruction.** By considering a conforming triangulation $\mathcal{T}^{h_N}$ of Ω, with characteristic length h_N, to be a set of finitely many triangular cells[1] $T_p \subset \Omega$, $p = 1, 2, \ldots, N$, we construct FV approximations on each T_p, see Fig. 1. Flow variables are placed at the barycenter of T_p, and we denote the set of indices of the neighboring triangles of T_p by $K(p) := \{q \in \mathbb{N} \mid \partial T_p \cap \partial T_q \text{ is a face of } T_p\}$. Then the semi-discretized form of (1) over each T_p can be written as follows

$$|T_p| \frac{\partial \mathbf{U}_p}{\partial t} + \sum_{q \in K(p)} \mathcal{H}^\star(\mathbf{U}_p^L, \mathbf{U}_q^R) \cdot \mathbf{n}_q = 0, \tag{3}$$

where $|T_p|$ is the area of T_p, $\mathbf{n}_q$ is the outward normal vector and $\mathcal{H}^\star$ is the numerical flux vector at each face's midpoint M, evaluated using the left and right states existing at the two sides of M, denoted as $\mathbf{U}_p^L$ and $\mathbf{U}_q^R$. Although a one-point quadrature rule is used here the ideas presented next can be applied to high-order integration, e.g. using Gauss quadrature. In general, this numerical flux function can be calculated as an exact or approximate local solution of the Riemann problem posed at a cell's face. In this work, Roe's approximate Riemann solver and the HLLC one have been utilized.

[1] Our discussion is based on the cell-centered FV (CCFV) approach, but it also holds for node-centered FV when the word "cell" is simply replaced by the "control volume", C_P.

3.1. **Solution reconstruction and limiting procedure.** For achieving second-order spatial accuracy most FV implementations calculate the $\mathbf{U}_p^L$ and $\mathbf{U}_q^R$ values assuming that the solution varies linearly in each cell, starting from given average solution values of adjacent cells, i.e. MUSCL-type local reconstructions. Three choices exist for this reconstruction; primitive, conservative and characteristic variables. Here, reconstruction on primitive and conservative variables has been investigated. To prevent oscillations from developing in the solution by controling the total variation of the reconstructed field, slope limiting has to be applied. In the present work, an alternative approach, compared to these usually implemented in unstructured CCFV schemes is used following [2, 3] and is briefly repeated next for completeness. Strict monotonicity in the reconstruction is enforced by the use of edge-based limiter functions, usually reserved for node-centered FV schemes of the median-dual type [2]. One such limiter is the modified Van Albada-Van Leer which is differentiable for linearly varying flow variables. Continuous differentiability helps in achieving smooth transition between discontinuous jumps with first-order representation and sharp but continuous gradients which require second-order consistency.

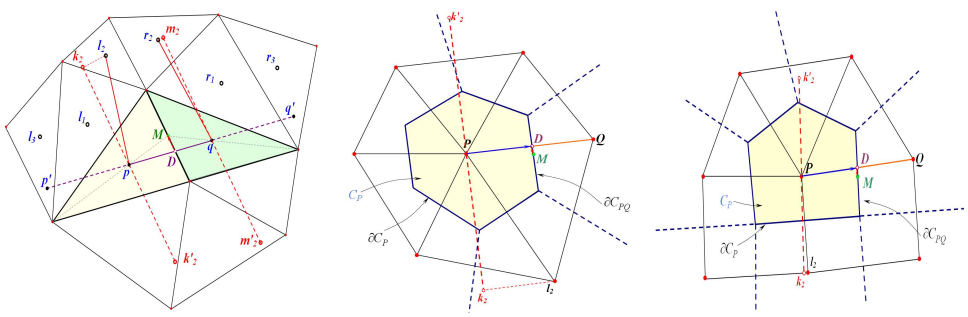

FIGURE 1. Cell-centered FV (left), centroid-dual FV (middle) and hybrid mesh (right)

Starting with a constant piecewise approximation of the $i-$th component of $\mathbf{W}_p$ (representing either primitive or conservative variables) and since we wish to apply edge-based limiters, one is forced to compute reconstructed values at the intersection point D of face $\partial T_q \cap \partial T_p$ and $\overline{pq}$, see Fig. 1, as to compare with the reference gradient value $w_{i,q} - w_{i,p}$. This choice seems natural also from a geometrical point of view since it corresponds to the linear interpolation between p and q. Therefore, we start by computing left and right extrapolated values at D as,

$$(w_{i,p})_D^L = w_{i,p} + \mathbf{r}_{pD} \cdot \nabla w_{i,p} \quad \text{and} \quad (w_{i,q})_D^R = w_{i,q} - \mathbf{r}_{Dq} \cdot \nabla w_{i,q}, \tag{4}$$

where $\mathbf{r}$ is a position vector relative to the centroid of the cell and $\nabla(\cdot)$ a gradient operator. Note that point D does not coincide, in general, with the face's midpoint M. Then a limiter function, $\Phi(\cdot,\cdot)$, has to be applied and its arguments have to be consecutive gradients of the solution defined in an upwind manner around face $\partial T_q \cap \partial T_p$. Thus, a virtual value q' has to be defined as a node upwind of q. The main difficulty now lies in the need to define this virtual q' value (similar we can define a p' value for p). We first denote the local centered reference gradient as $(\nabla w_{i,q})^{\text{cnt}} \cdot \mathbf{r}_{pq} = w_{i,q} - w_{i,p}$, and we compute the upwind gradient $w_{i,q} - w_{i,q'}$ by

expressing the virtual unknown q' value using known ones by assuming that q' is chosen such that it lies along edge $\overline{pq}$ and that q is at the center of $\overline{pq'}$. In this case,

$$\begin{aligned} w_{i,q'} - w_{i,q} &= (w_{i,q'} - w_{i,p}) - (w_{i,q} - w_{i,p}) = (\nabla w_{i,q}) \cdot \mathbf{r}_{pq'} - (w_{i,q} - w_{i,p}) \\ &= 2\,(\nabla w_{i,q}) \cdot \mathbf{r}_{pq} - (\nabla w_{i,q})^{\text{cnt}} \cdot \mathbf{r}_{pq}. \end{aligned}$$

Then, to invoke monotonicity, limiting is performed and the ratio of the corresponding lengths has to be used, resulting in the left and right states at face $\partial T_q \cap \partial T_p$ as

$$(w_{i,q})_D^R = w_{i,q} - \frac{||\mathbf{r}_{Dq}||}{||\mathbf{r}_{pq}||} \Phi \left((\nabla w_{i,q})^{\text{upw}} \cdot \mathbf{r}_{pq}, (\nabla w_{i,q})^{\text{cnt}} \cdot \mathbf{r}_{pq} \right); \tag{5}$$

$$(w_{i,p})_D^L = w_{i,p} + \frac{||\mathbf{r}_{pD}||}{||\mathbf{r}_{pq}||} \Phi \left((\nabla w_{i,p})^{\text{upw}} \cdot \mathbf{r}_{pq}, (\nabla w_{i,p})^{\text{cnt}} \cdot \mathbf{r}_{pq} \right), \tag{6}$$

where the upwind limiter arguments are given as

$$(\nabla w_{i,q})^{\text{upw}} = 2\nabla w_{i,q} - (\nabla w_{i,q})^{\text{cnt}} \quad \text{and} \quad (\nabla w_{i,p})^{\text{upw}} = 2\nabla w_{i,p} - (\nabla w_{i,p})^{\text{cnt}}.$$

In an ideal unstructured grid the variables are extrapolated to the center M of a cell's face and as such the numerical integration of the exact flux with the midpoint rule will be exact for linear functions along $\partial T_q \cap \partial T_p$. If the variables are extrapolated to a different location, e.g. at point D, then the one-point interpolation is expected to be only first-order accurate, especially for types of grids where the distance between optimal location M and the extrapolated location D is large [4, 2, 3]. This inconsistency had to be corrected thus, a correction was proposed and tested for smooth shallow water flow conditions in [2]. Hence, after the reconstructed values (5) and (6) at D have been computed, a directional correction is applied in order to compute reconstructed values at M, as follows,

$$(w_{i,p})_M^L = (w_{i,p})_D^L + \mathbf{r}_{DM} \cdot \nabla w_{i,p} \quad \text{and} \quad (w_{i,q})_M^R = (w_{i,q})_D^R + \mathbf{r}_{DM} \cdot \nabla w_{i,q}. \tag{7}$$

Since the gradient estimates used in the above correction terms are unlimited it was shown that, accurate gradient computations would result in an accurate correction, in the sense of retaining second order accuracy for smooth flows, on poor connected grids where the distance between D and M is large [2], even for highly stretched meshes. However, further considerations had to be taken into account if shocks are to be present in the flow field. As such, the correction terms in (7) have to be properly limited along the direction of $\overline{DM}$ as proposed in [3], thus enhancing the multidimensional character of the reconstruction. Achieving this is not trivial since proper reference values have to be defined, as to calculate limiter arguments that are physically meaningful. Assuming we want to properly limit the directional correction added to $(w_{i,p})_M^L$ in (7), we first identify the set of indices $l_j, j = 1, 2, 3$ of the triangles T_{l_j} that have now a common vertex with T_p in the direction of $\overline{DM}$. We choose as a reference triangle the one for which $\overline{pl_j}$ has the smallest angle with $\overline{DM}$, which is T_{l_2} in Fig. 1, and project its cell center in the direction of $\overline{DM}$, with $\overline{pk_2}$ being that projection. Now, the extrapolated value at k_2 is calculated from the value at the barycenter l_2 as

$$w_{i,k_2} = w_{i,l_2} + \mathbf{r}_{l_2 k_2} \cdot \nabla w_{i,l_2}.$$

We can now define the local central reference gradient as $(\nabla w_{i,p})^{\text{cnt}} \cdot \mathbf{r}_{pk_2} = w_{i,k_2} - w_{i,p}$, and compute the upwind gradient $w_{i,p} - w_{i,k_2'}$ by expressing the virtual

unknown k_2' value using known values as detailed before. This leads to the left reconstructed value (now corrected and limited) at the flux integration point M,

$$(w_{i,p})_M^L = (w_{i,p})_D^L + \frac{||\mathbf{r}_{DM}||}{||\mathbf{r}_{pk_2}||}\Phi\left((\nabla w_{i,p})^{\text{upw}} \cdot \mathbf{r}_{pk_2}, (\nabla w_{i,p})^{\text{cnt}} \cdot \mathbf{r}_{pk_2}\right), \quad (8)$$

where now

$$(\nabla w_{i,p})^{\text{upw}} = 2\nabla w_{i,p} - (\nabla w_{i,p})^{\text{cnt}}.$$

With similar reasoning, the right limited reconstructed value at M is computed as

$$(w_{i,q})_M^R = (w_{i,q})_D^R + \frac{||\mathbf{r}_{DM}||}{||\mathbf{r}_{qm_2}||}\Phi\left((\nabla w_{i,q})^{\text{upw}} \cdot \mathbf{r}_{qm_2}, (\nabla w_{i,q})^{\text{cnt}} \cdot \mathbf{r}_{qm_2}\right). \quad (9)$$

Similar rationale can be followed to correct the inconsistency between points D and M for node-centered FV schemes of the centroid-dual type, as depicted in Fig. 1.

Finally, it remains to define appropriate gradient operators for the reconstruction presented above for the CCFV approach. Here, the gradient is computed in the closed path defined for every T_p by connecting the barycenters of the triangles having a common vertex with T_p, taking into account the assumption that the gradient is constant, i.e. Green-Gauss (GG) linear reconstruction. As it was demonstrated in [3], when this (wide) stencil is used for gradient computations an almost identical convergence behavior is achieved on different grid types, with no reduction on the asymptotic convergence rate while for steady-state calculations convergence is greatly improved. This is due to the fact that the data points involved in this gradient computation satisfy the so-called good neighborhood for Van Leer limiting.

4. **Numerical Tests and Results.** In our scheme, named CCFVw2L, the Van Albada-Van Leer limiter was implemented on the tests to follow, while a second-order explicit SSP Runge-Kutta time integration is used under the usual CFL stability condition for the time step computation. Ghost cells are implemented for boundary treatment. To test performance and convergence properties regular and irregular grids, shown in Fig. 2, have been used. These grids exhibit different connectivity behaviors for internal and boundary cells [3]. Comparisons between the results obtained with the Venkatakrishnan [7] V-limiter and the MLPu2 [6] one are also presented. It is noted that, these two truly multidimensional limiters have a tunable parameter[2], K, that is problem dependent and needs to be carefully chosen.

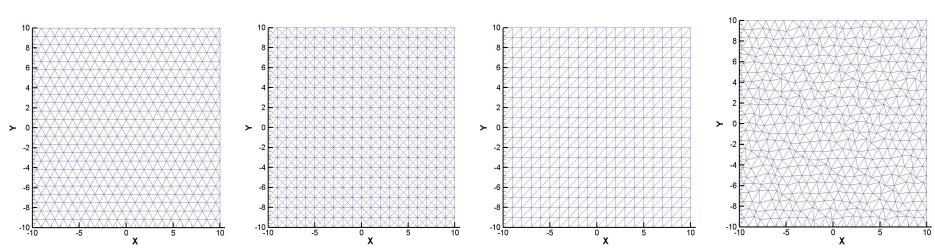

FIGURE 2. Regular and irregular grids: types I-IV from left to right

[2]If $K = 0$ the limiter is always active, and strict monotonicity is maintained, while a very large value of K essentially means no limiting and monotonicity is violated.

4.1. **Isentropic Vortex Problem.** This 2D vortex problem is often used as a benchmark for comparing numerical methods for fluid dynamics. The flow-field is smooth and the exact solution is known. The mean flow is with $\rho_\infty = 1, p_\infty = 1$, and $[u_\infty, v_\infty]^{\mathrm{T}} = [1, 1]^{\mathrm{T}}$ in a domain $\Omega = [-10, 10] \times [-10, 10]$ with periodic boundary conditions. An isentropic vortex is added [6, 5] and the exact solution of the problem is the initial solution shifted by $(u_\infty t, v_\infty t)$ thus, numerical phase (dispersion) and amplitude (dissipation) errors are easy to identify. Roe's Riemann solver is implemented for this test case applying reconstruction on the primitive variables. In Fig. 3 the density contours of computed solutions compared with the exact solution at time $t = 2T$ are presented for the CCFVw2L scheme and those using the V and MLPu2 limiters with $K = 5$ on a type-IV distorted grid. Next and in Fig 4 we report grid convergence studies on all different grids, having been consistently refined.

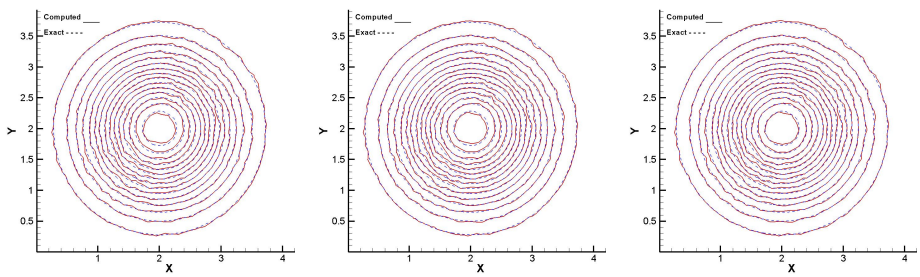

FIGURE 3. Isentropic vortex at $t = 2T$: V-limiter (left), MLPu2 (middle) and CCFVw2L (right)

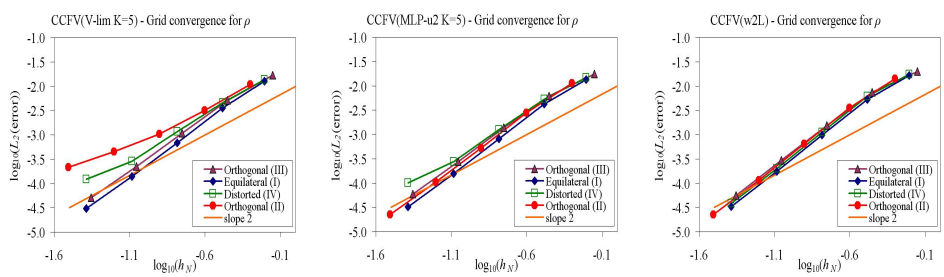

FIGURE 4. Isentropic vortex: convergence results on all grid types

4.2. **Shock tube problems.** These (one-dimensional in nature) test cases are chosen as to test the capability of the proposed methodology in resolving various linear and non-linear waves on unstructured grids. The computational domain is $[0, 1] \times [0, 0.1]$ with a triangulation of $N = 16,000$ cells on a type-II mesh. Three cases are considered, namely, (a) Sod's problem, (b) Harten-Lax problem and (c) Supersonic expansion, with Riemann-type initial conditions given respectively as

(a) $(\rho_L, u_L, v_L, p_L) = (1, 0, 0, 1)$ and $(\rho_R, u_R, v_R, p_R) = (1, 0, 0, 1)$,

(b) $(\rho_L, u_L, v_L, p_L) = (0.445, 0.698, 0, 3.528)$ and $(\rho_R, u_R, v_R, p_R) = (0.5, 0, 0, 0.571)$,

(c) $(\rho_L, u_L, v_L, p_L) = (1, -2, 0, 0.4)$ and $(\rho_R, u_R, v_R, p_R) = (1, 2, 0, 0.4)$

and the HLLC approximate Riemann solver is used in all problems applying reconstruction on the conservative variables. Comparisons between the proposed CCFVw2L scheme and the MLPu2 are shown in Fig. 5.

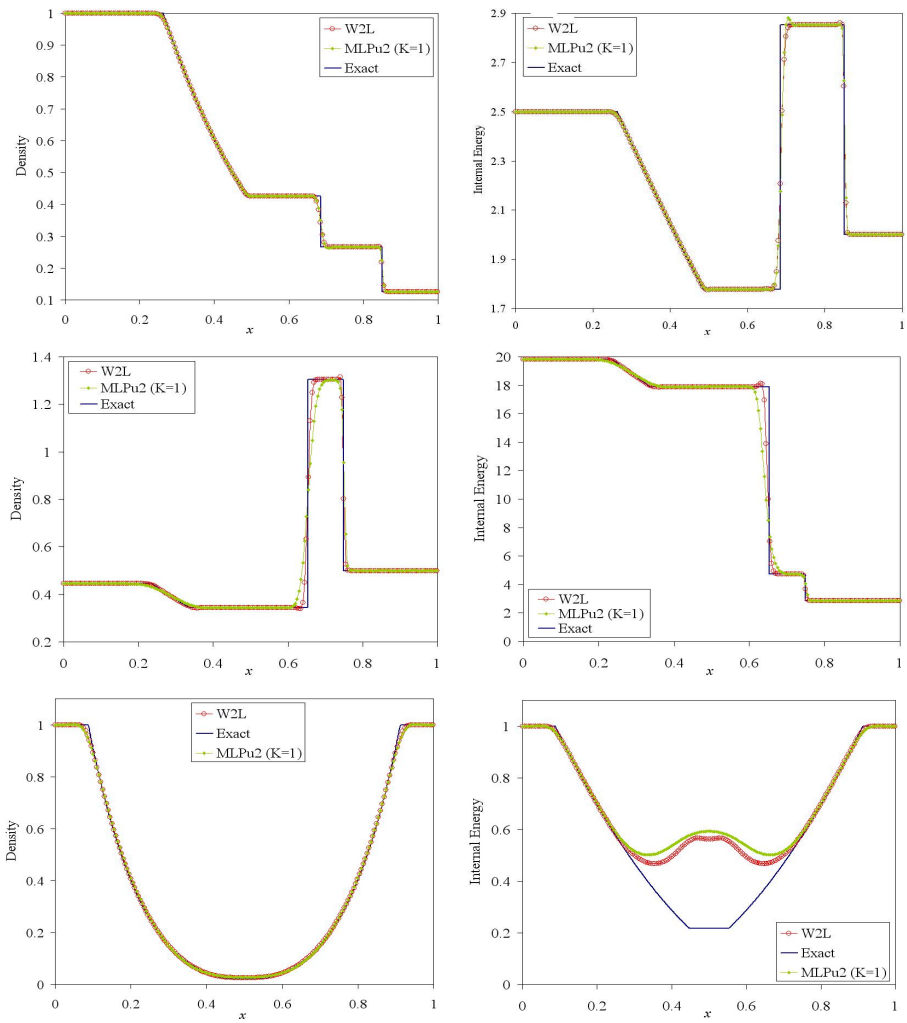

FIGURE 5. Shock tube problems: Sod problem (top), Lax problem (middle) and supersonic expansion problem (bottom)

4.3. **Transonic flow around NACA 0012 airfoil.** The case of transonic flow around NACA 0012 airfoil is considered here with Mach number number 0.8 and $\alpha = 1.25°$ as to obtain a convergent solution. The number of triangular cells used was $N = 6,492$ with 200 surface grid points. The grid and convergence history obtained using the HLLC solver and reconstruction on the primitive variables are shown in Fig. 6 while Fig. 7 shows a comparison of the surface pressure coefficient between the CCFVw2L and MLPu2 schemes.

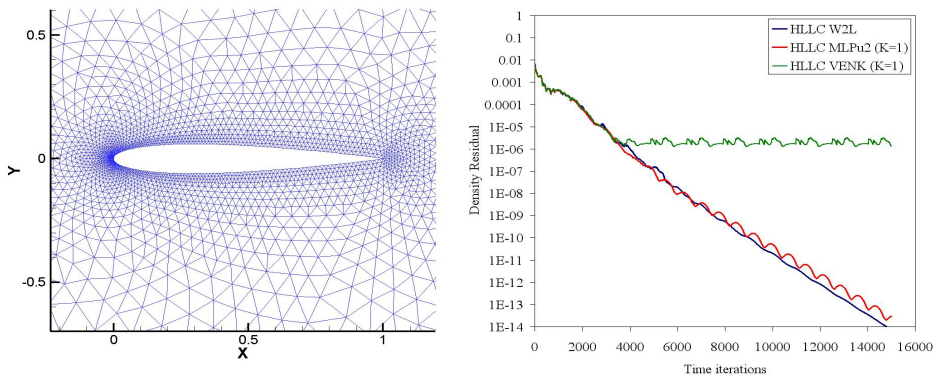

FIGURE 6. Grid distribution and convergence history (NACA0012 airfoil)

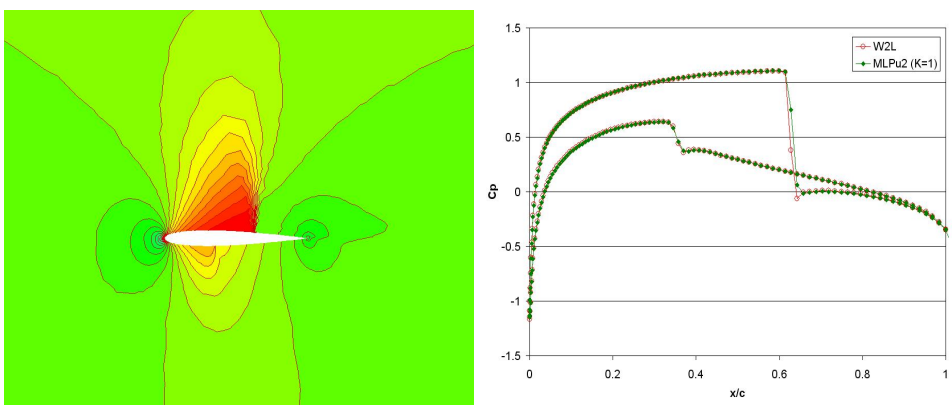

FIGURE 7. Mach contours and surface pressure over NACA0012 airfoil

REFERENCES

[1] S. Clain and V. Clauzon, *Monoslope and multislope MUSCL methods for unstructured meshes*, J. Comp. Phys., **229** (2010), 3745–3776.

[2] A. I. Delis, I.K. Nikolos and M. Kazolea, *Performance and comparizon of cell-centered and node centered unstructured finite volume discretizations for shallow water free surface flows*, Archives of Computational Methods in Engineering, **18** (2011), 57–108.

[3] A. I. Delis and I.K. Nikolos, *A novel multi-dimensional solution reconstruction and edge-based limiting procedure for unstructured cell-centered finite volumes with application to shallow water dynamics*, Int. J. Numer. Meth. Fluids, **71** (2013), 584-633.

[4] M.E. Hubbard, *Multi-dimensional slope limiters for MUSCL-type finite volume schemes on unstructured grids*, J. Comp. Phys., **155** (1999), 54–74.

[5] W. Li, Y.-X. Ren G. Lei and H. Luo, *The multi-dimensional limiters for solving hyperbolic conservation laws on unstructured grids*, J. Comp. Phys., **230** (2011), 7775-7795.

[6] J.S. Park, S.-H. Yoon and C. Kim, *Multi-dimensional limiting process for hyperbolic conservation laws on unstructured grids*, J. Comp. Phys., **229** (2010), 788-812.

[7] V. Venkatakrishan, *Convergence to steady state of the Euler Equations on unstructured grids with limiters*, J. Comp. Phys., **118** (1995), 120-130.

Received xxxx 20xx; revised xxxx 20xx.

E-mail address: `adelis@science.tuc.gr`
E-mail address: `jnikolo@dpem.tuc.gr`